Polymeric Hydrate−Inhibitor Adsorption Measured by Neutron Scattering

Jeffrey L. Hutter,† H. E. King, Jr.,* and Min Y. Lin‡

Exxon Mobil Research and Engineering Company, Annandale, New Jersey 08801

Received June 8, 1999; Revised Manuscript Received December 13, 1999

ABSTRACT: We use small-angle neutron scattering to characterize a polymeric hydrate inhibitor, poly(*N*-vinyl-2-pyrrolidone), adsorbed onto hydrate crystal surfaces. Gas hydrates are crystals in which water molecules encage small molecules such as propane or methane. Their stability at temperatures above the freezing point of water presents a significant challenge to oil and gas transport. Hydrate formation can be kinetically suppressed by certain polymeric inhibitors, but little is known about the mechanism of this effect. We measure a polymer coverage of 5 ± 3 mg/m^2, but on only a small (2%) fraction of the available surface. Unlike the expected self-similar structure seen in other systems, this layer has the unusual property of a thickness several times the polymer coil dimension. Therefore, most of the polymer is not bound directly to the surface, suggesting the formation of surface aggregates. We speculate on the role of these aggregates in the growth inhibition of hydrate crystals.

I. Introduction

Gas hydrates are ice-like crystals consisting of water cages surrounding small molecules such as propane or methane.[1] Enclathration of the small molecules is key to the crystals' stability, and depending upon the gas pressure, their melting point can extend to temperatures well above the ice freezing point. Because of this, they crystallize in many settings where ordinary ice is not stable. For example, there are many natural-gas hydrate deposits on the sea floor associated with gas seepage into cold ocean water.[2] Similar conditions can be found inside oil and gas transport pipelines, and hydrate formation is a significant long-standing problem for the oil industry.[3] The consequences of hydrate formation inside deep-sea pipelines can be very serious. It is possible for the pipeline to become permanently blocked or for attempts to release the hydrate plug to cause serious accidents: the solid plug can be propelled through the pipeline by a high differential pressure. These are sufficiently serious consequences that there is great interest in preventing hydrate formation. In addition to installing thermally insulated pipelines, a common approach has been to add an antifreeze compound, typically methanol, to lower the formation temperature.[3] This approach has drawbacks such as the requirement for high volume fractions of methanol (up to 50 vol %) and the potential environmental impact of spillage. There are also considerable costs associated with supply and recovery of the methanol.

An alternative to thermodynamic suppression is kinetic inhibition. Recently it has been found that certain water-soluble polymers can kinetically inhibit hydrate formation.[4] Experiments show that, at the less than 1 wt % concentration where these polymers are utilized, there is little shift in the equilibrium hydrate formation point. But they inhibit hydrate formation by several degrees during continuous cooling and suppress crystallization for long time periods at intermediate levels of subcooling. These laboratory tests were sufficiently promising to encourage tests in actual pipelines, where indications are positive.[5]

Despite these technical achievements, the mechanism of inhibition remains unclear.[6,7] From studies of polymer conformation in dilute aqueous solution (at the concentration of use), there is little to distinguish a hydrate-inhibiting polymer such as poly(*N*-vinyl-2-pyrrolidone), hereafter PVP, from a typical nonionic water-soluble polymer such as polyethylene oxide, hereafter PEO. Light-scattering studies show that both exhibit classic "good-solvent" behavior.[8] Addition of small amounts of hydrate-forming molecules such as tetrahydrofuran (THF) do not alter this.[9] At higher polymer concentrations, in the semidilute (chain-overlap) regime, PVP does exhibit some anomalous solution behavior—a self-aggregation occurs. These solution properties, though unusual, are not obviously related to the inhibitor function.

The characteristic features of polymeric hydrate inhibitors are their ability to slow hydrate growth velocity and alter the consequent morphology. Structure II hydrate crystals normally grow as faceted, nearly-symmetric octahedra,[10] but upon addition of a hydrate-inhibitor polymer they grow as plates.[6,11] The aspect ratio of these plates is large—crystals ~25 μm thick can form plates 1 mm across. This modification is surprising because the platelike crystals are bounded by the same eight, crystallographically equivalent planes as are the octahedra. Thus, unlike conventional crystal habit modifiers, which alter the crystal shape by suppressing growth of a particular crystallographic plane, the inhibitor polymers apparently alter the growth in some other fashion. For a platelike crystal this amounts to either the suppression of growth on two parallel faces of the proto-octahedra or the acceleration of growth on the six bounding faces.

In a companion paper,[12] we present small-angle neutron scattering (SANS) studies of THF/water hydrates grown in the presence of both inhibitor and noninhibitor polymers. For the inactive polymers, such as PEO, we found that the polymer remains in solution,

† Present address: Department of Physics and Astronomy, University of Western Ontario, London, Ontario N6A 3K7, Canada.
‡ Also at the National Institute of Standards and Technology, Gaithersburg, MD 20899.
* To whom correspondence should be addressed.

10.1021/ma990912p CCC: $19.00
Published on Web 03/09/2000

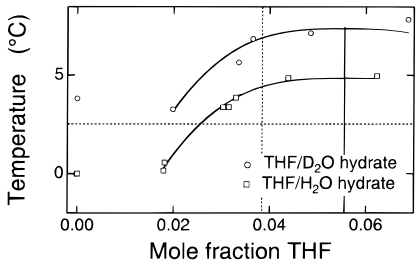

Figure 1. Partial phase diagram for THF hydrates. We include data from Hanley (ref 14) for the coexistence of THF hydrates with liquid solution. The curves represent the liquidus. Vertical solid line: 1:17 stoichiometric composition for hydrates with a THF filling fraction of 1. Vertical dashed line: composition used in our studies. Horizontal dashed line: temperature used in our studies. In our experiments, the solid fraction is approximately 0.5, as explained in the text.

apparently not interacting with the hydrate crystals. On the other hand, inhibitor polymers such as PVP and poly(vinylcaprolactam) (PVCap) show additional scattering from an adsorbed layer. However, due to the simultaneous contribution of several structure factors to the measured signal, the amount of adsorbed polymer could not be reliably determined.

In the present work, we select one of the active polymers—PVP—for further study in a contrast variation SANS experiment. Contrast variation provides the ability to isolate the various structure factors, allowing us to independently measure the hydrate surface area and total amount of polymer adsorbed. Thus, we are able to measure details of the adsorbed polymer layer that will lead to a better understanding of the mechanism of crystal growth modification.

II. Experimental Section

A. Sample Preparation. Several molecules can form hydrates with water. In our studies, we use a solution of THF in water. THF is convenient because it is a water-soluble liquid and forms structure II hydrates at a temperature of about 5 °C at atmospheric pressure. These crystals have a cubic lattice with edge length $a = 17.24$ Å and an idealized formula THF·$17H_2O$. However, the molar ratio need not be 1:17 over the entire stability range. The THF/water hydrate has been studied by two groups.[13,14] The earlier study concludes that the filling fraction of THF is at least 98%, while the later study places it at 99.9%. We use the latter value in our calculations.

For our experiments we utilize an off-composition molar ratio of 1:25 THF to water, which allows us to create a partially frozen slurry consisting of hydrate crystals and THF-depleted solution. Figure 1 shows partial phase diagrams for THF hydrates of both normal and deuterated water. The data points are taken from Hanley[14] and show coexistence conditions for both hydrates with their respective liquids. The D_2O hydrates have an equilibrium melting point ~3 °C higher than that of H_2O hydrates. Not shown is a eutectic point at a composition of <0.02 mol fraction THF.

We prepared samples with a 1:25 mole ratio of 99.5% deuterated THF[15] (hereafter, TDF) to water. We varied the D_2O level for our experiments over a range of 0.8−1 mole fraction by mixing two such solutions, one containing D_2O[16] and one H_2O. Addition of 0.5 wt % polymer resulted in the solutions used for the experiments. We chose poly(*N*-vinyl-2-pyrrolidone) (PVP) as a typical hydrate inhibitor. Our PVP sample was the same as that characterized by Sun and King[8] and has $M_w = 49\,000$ g/mol. The resulting solution compositions are summarized in Table 1.

Once prepared, the solutions were transferred to standard quartz banjo cells 0.5 cm thick and 2 cm in diameter. We added a magnetic stir bar to each cell to allow agitation during crystallization. Cooling to the desired temperature in a water bath produced partially frozen samples. Often, we needed to nucleate the hydrate phase by locally cooling the sample with a cold point. Continuous stirring during the freezing process resulted in a roughly uniform distribution of crystals approximately 40 μm across (as measured by optical microscopy) surrounded by the TDF-depleted solution.[17] We then transferred the samples to a controlled temperature stage mounted on the beamline.

Table 1. Compositions of Samples

sample	mole ratio TDF:water	water deuteration	mole ratio monomer:solvent
1	0.03992 ± 0.00003	0.7946 ± 0.0002	0.00100 ± 0.00004
2	0.03993 ± 0.00003	0.8994 ± 0.0002	0.00101 ± 0.00003
3	0.03993 ± 0.00003	0.9575 ± 0.0001	0.00100 ± 0.00003
4	0.03993 ± 0.00003	0.9788 ± 0.0001	0.00101 ± 0.00003
5	0.03993 ± 0.00003	0.999 ± −	0.00101 ± 0.00003

B. Small-Angle Neutron Scattering Experiments. The small-angle neutron scattering measurements were performed at the Center for Neutron Research, National Institute of Standards and Technology in Gaithersburg, MD. We measured data over a scattering wavevector (q) range of $0.0025 < q < 0.2$ Å^{-1}. This was accomplished at the NG3-SANS beamline using a neutron wavelength of 7 Å and two overlapping q ranges with sample−detector distances of 2.7 and 13 m. Scattering signals I_s were recorded by a 2D area detector. Data reduction followed the procedure described in the NIST SANS data reduction manual.[18] Measured scattering from the empty sample cell I_c and background I_b is subtracted via the formula

$$I' = I_s - I_b - \frac{T_s}{T_c}(I_c - I_b) \quad (1)$$

which accounts for attenuation of the scattered intensities by both cell and sample according to their measured neutron transmissions T_c and T_s, respectively. The 2D I' data is then corrected by a detector efficiency function and reduced to a 1D differential scattering cross section $d\sigma(q)/d\Omega$ by circularly averaging and referencing to a known standard.[19]

III. Results

A. Fully Deuterated Solvents. As previously discussed, we have performed similar scattering experiments using fully deuterated solvents.[12] We summarize relevant features of those experiments here. For the polymer-free slurries, the observed scattering is well described by a combination of the Porod scattering function, which has a q^{-4} dependence, plus a q-independent background. Scattering from a polymer-containing slurry gives a similar Porod contribution but also exhibits significant additional scattering at higher q values. In the case of a noninhibitor polymer, PEO, we find that this additional scattering is well described by a Debye-like form. Thus, the resulting scattering is the sum of two terms: that due to the crystal surfaces and that due to the polymer in solution. In the case of inhibitor polymers, there are two significant changes in the scattering from the slurry: First, the Porod scattering amplitude is considerably larger than that of the polymer-free or PEO samples. Second, the scattering amplitude at high q falls off more slowly than the Debye-like scattering seen for the same sample with no crystals present (at a slightly higher temperature). In the present work we utilize contrast variation to show that this excess scattering, both in the Porod regime and at higher q, arises from polymer adsorbed to the crystal surface.

B. Contrast Variation. The scattering from a sample in which polymer is partitioned between solution and surface represents the sum of three independent struc-

tures: Porod scattering from interfaces, Debye scattering from solvated polymer, and scattering from the adsorbed polymer layer. For the case of an adsorbed layer with no polymer remaining in solution, Auvray and co-workers have modeled scattering due to the interfaces and adsorbed layer as[20,21]

$$I_{\mathrm{coh}}(q) = (n_{\mathrm{g}} - n_{\mathrm{s}})^2 S_{\mathrm{gg}}(q) - 2(n_{\mathrm{g}} - n_{\mathrm{s}})(n_{\mathrm{p}} - n_{\mathrm{s}}) S_{\mathrm{pg}}(q) + (n_{\mathrm{p}} - n_{\mathrm{s}})^2 S_{\mathrm{pp}}(q) + B \quad (2)$$

where n_{g}, n_{s}, and n_{p} are the scattering length densities of the solid, pure solvent, and polymer, respectively. Here, S_{gg}, S_{pg}, and S_{pp} denote the solid−solid, solid−polymer, and polymer−polymer partial structure factors, and B is a background taken to be independent of q—but not n_{s}—over the q range accessible by our experiment.

The structure factor S_{gg} is the well-known Porod scattering from surfaces and has the form

$$S_{\mathrm{Porod}}(q) = 2\pi(S/V)q^{-4} \quad (3)$$

where S/V is the interfacial surface area per unit scattering volume (provided that $q \gg 1/R$, where R is the radius of curvature of the surface—a good assumption for our faceted crystals).

The polymer−polymer structure factor S_{pp} consists of a term sensitive to the average profile $\langle\phi(z)\rangle$ of the polymer layer (as a function of distance z from the interface),

$$\bar{S}_{\mathrm{pp}}(q) = 2\pi(S/V)q^{-2}\left|\int_0^\infty \mathrm{d}z\langle\phi(z)\rangle \mathrm{e}^{iqz}\right|^2 \quad (4)$$

and a term $\tilde{S}$ which takes into account local deviations from the average profile.

Finally, the interference term S_{pg} is proportional to the Fourier sine transform of the profile:

$$S_{\mathrm{pg}}(q) = 2\pi(S/V)q^{-3}\int_0^\infty \mathrm{d}z\langle\phi(z)\rangle \sin qz \quad (5)$$

Equation 2 neglects the scattering from polymer in solution. Because the solvated and adsorbed polymer scatter incoherently, the solution scattering term may be simply added to the others in eq 2. We model this scattering as the Debye-like structure factor

$$\hat{S}_{\mathrm{Beaucage}}(q) = G[\exp(-q^2 R_{\mathrm{g}}{}^2/3) + d_{\mathrm{f}}\Gamma(d_{\mathrm{f}}/2)/(R_{\mathrm{g}}q^*)^{d_{\mathrm{f}}}] \quad (6)$$

due to Beaucage,[22] where $q^* = q/[\mathrm{erf}(kqR_{\mathrm{g}}/\sqrt{6})]^3$ with $k \approx 1.06$. Fitting our data to this form allows us to extract the polymer radius of gyration R_{g} and the fractal dimension d_{f} of the polymer coils (an indicator of solvent quality) from the data. The Guinier prefactor G is approximately proportional to the concentration of polymer chains, and $\Gamma(n)$ is the gamma function.

A powerful feature of neutron scattering is the ability to vary scattering contrasts through changes in the isotopic content. One can make use of this to extract the partial structure factors of interest in eq 2. Through a series of m experiments with different (known) contrasts, m linear equations for the three partial structure factors are obtained:

$$\begin{pmatrix} (n_{\mathrm{g}}^{(1)} - n_{\mathrm{s}}^{(1)})^2 & -2(n_{\mathrm{g}}^{(1)} - n_{\mathrm{s}}^{(1)})(n_{\mathrm{p}}^{(1)} - n_{\mathrm{s}}^{(1)}) & (n_{\mathrm{p}}^{(1)} - n_{\mathrm{s}}^{(1)})^2 \\ \vdots & & \\ (n_{\mathrm{g}}^{(i)} - n_{\mathrm{s}}^{(i)})^2 & -2(n_{\mathrm{g}}^{(i)} - n_{\mathrm{s}}^{(i)})(n_{\mathrm{p}}^{(i)} - n_{\mathrm{s}}^{(i)}) & (n_{\mathrm{p}}^{(i)} - n_{\mathrm{s}}^{(i)})^2 \\ \vdots & & \\ (n_{\mathrm{g}}^{(m)} - n_{\mathrm{s}}^{(m)})^2 & -2(n_{\mathrm{g}}^{(m)} - n_{\mathrm{s}}^{(m)})(n_{\mathrm{p}}^{(m)} - n_{\mathrm{s}}^{(m)}) & (n_{\mathrm{p}}^{(m)} - n_{\mathrm{s}}^{(m)})^2 \end{pmatrix} \times \begin{pmatrix} S_{\mathrm{gg}}(q) \\ S_{\mathrm{pg}}(q) \\ S_{\mathrm{pp}}(q) \end{pmatrix} + \begin{pmatrix} B^{(1)} \\ \vdots \\ B^{(i)} \\ \vdots \\ B^{(m)} \end{pmatrix} = \begin{pmatrix} I^{(1)}(q) \\ \vdots \\ I^{(i)}(q) \\ \vdots \\ I^{(m)}(q) \end{pmatrix} \quad (7)$$

Here, $n_\alpha^{(i)}$ is the scattering length density of component α in experiment i. One then solves eq 7 for the structure factors. This contrast variation technique has proved useful for the measurement of adsorbed polymer layers.[21]

We performed SANS measurements for five samples (Table 1) with differing H_2O/D_2O ratios, each containing 0.5 wt % of PVP. Since the scattering length density of hydrogen is very different from that of deuterium, this results in significant variation in n_{s} and n_{g}. Thus, we have an overdetermined set of equations which we solve, in the least-squares sense, for the individual partial structure factors, using the method of singular value decomposition (SVD).[23]

Our experiment differs in two important ways from previous SANS studies of polymer adsorption.[21,24] First, we form our surfaces by in situ solidification. Thus, although the volume *fraction*[25] of solid is fixed by the temperature, the surface area is not a priori fixed and could vary from sample to sample. Our experimental procedure minimizes this variation by thorough stirring of the slurries during crystallization. Confirmation of the effectiveness of this is seen in our measurements of the surface area through the Porod amplitude (see Appendix A4), which indicate little variation among the samples. Second, much of the polymer remains in solution, resulting in a large contribution to the scattering. Equation 2 must therefore be modified in two ways. As discussed, we add a fourth term describing this scattering. We must also adjust the solution scattering length density, n_{s}, to account for the presence of polymer (see Appendix A1).

To solve eq 7, we need accurate estimates of the contrasts in the coefficient matrix. We obtain these in two steps. First, we use the scattering length densities and concentrations of the materials in the prepared samples to calculate the expected contrast, and then we use experimental constraints to refine this estimate. Details are included in the Appendix.

C. Contrast Variation Measurement of the Polymer Solution Structure Factor. Armed with estimates of the contrast factors, we can now proceed to measure the structure factors. First, we consider scattering from the polymer solutions at 7 °C. There are no hydrate crystals present at this temperature, and therefore no adsorbed layer, so the coefficient matrix eq 7 simplifies to a single column $(n_{\mathrm{p}} - n_{\mathrm{s}})^2$ multiplying the structure factor S_{pp}. To solve eq 7, we require the background vector $\bar{B}$, which we obtain by extrapolation of the high-q data for each of the five data sets. Solving the simplified eq 7 yields the structure factor shown in Figure 2. An indication of the accuracy of the decomposition is that the resulting points show a smooth variation with q although the SVD method imposes no relation among the points.

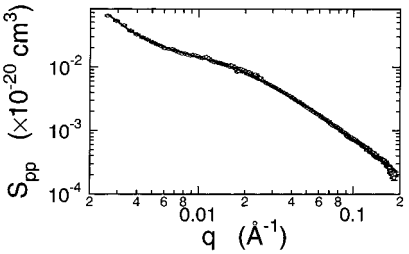

Figure 2. Structure factor S_{pp} for polymer in solution at 7 °C. The curve is a fit to eq 6.

The fit to the Beaucage form (eq 6) shown in Figure 2 measures properties of the solvated polymer. The resulting radius of gyration is $R_g = 82 \pm 5$ Å, similar to the hydrodynamic radius $R_H = 77$ Å determined from dynamic light scattering.[8] The fractal dimension d_f of the polymer coils obtained from the fit is 1.77 ± 0.05, similar to the fractal dimension of a self-avoiding random-walk value of $^5/_3 \approx 1.67$, which one would expect for this good solvent system.[26] We expect the amplitude G of the polymer scattering to be approximately proportional to the polymer concentration c according to[27]

$$G = c/\rho_p{}^2 N_A\left(\frac{1}{W_{poly}} + 2A_2c\right) \qquad (8)$$

Here, W_{poly} is the molecular weight of the polymer and A_2 is the second virial coefficient. Using the values of $W_{poly} = 49\,000 \pm 300$ g/mol and $A_2 = (8.4 \pm 1.0) \times 10^{-4}$ mol cm^4/g^2 determined by Sun and King[8] for our polymer sample, and our concentration of 5.56 g/L, we predict a value of $G = (1.9 \pm 0.2) \times 10^{-22}$ cm^3, which is somewhat higher than the value of $(1.54 \pm 0.01) \times 10^{-22}$ cm^3 measured by the fit. A similar scattering deficit has been noted for other water-soluble polymers, e.g. PEO.[28]

In addition to the expected polymer scattering modeled by eq 6, the data in Figure 2 exhibit an intensity excess at low q. This scattering is also evident in the raw data.[12] Such low-q tails have been previously noted for water-soluble polymers,[8,29] where they have been attributed to dust or other contamination in solution.[30] However, because the scattering intensity here has the same dependence on the deuterated fraction of water as does the polymer, we conclude that it arises from the polymer itself.[31] Aggregation of a small fraction of the polymer would help explain the deficiency between the measured and predicted value of G. Various power-law exponents can adequately fit the low-q tail; we use a $q^{-2.5}$ power law.

D. Measurement of the Partial Structure Factors for the Slurry State. For the case of interest in this study—partially frozen polymer solutions—we require the contrast of both hydrate crystal and polymer with the *average* solution. Using eq A5, we estimate contrast matching points of $x_{g\bar{s}} = 0.966$ and $x_{p\bar{s}} = 0.216$. As shown in Figure 3, each of the contrast factors in eq 2 varies quadratically with f_{D_2O}. Both the position and amplitude of the parabolae are important: the differing dependencies on f_{D_2O} enable the SVD method to separate the terms, while the absolute amplitudes allow one to extract numerical values of quantities such as the surface area.

Using the contrasts shown in Figure 3 and a background vector $\bar{B}$ obtained from extrapolations of the five individual data sets, we calculate the partial structure factors S_{gg}, S_{pp}, and S_{pg}.[32] Results are plotted in Figures 4 and 5b.

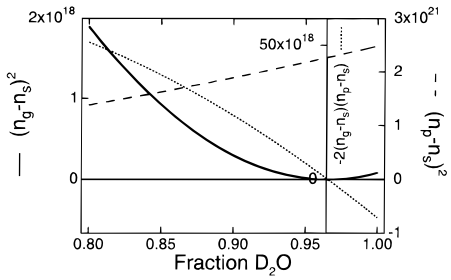

Figure 3. Contrasts (in units of cm^{-4}) as a function of f_{D_2O}. Shown on three separate axes are the hydrate-average solution contrast $(n_g - n_s)^2$, polymer-average solution contrast $(n_p - n_s)^2$, and the cross-term $-2(n_g - n_s)(n_p - n_s)$. Note that the latter term crosses zero at x_{gs}.

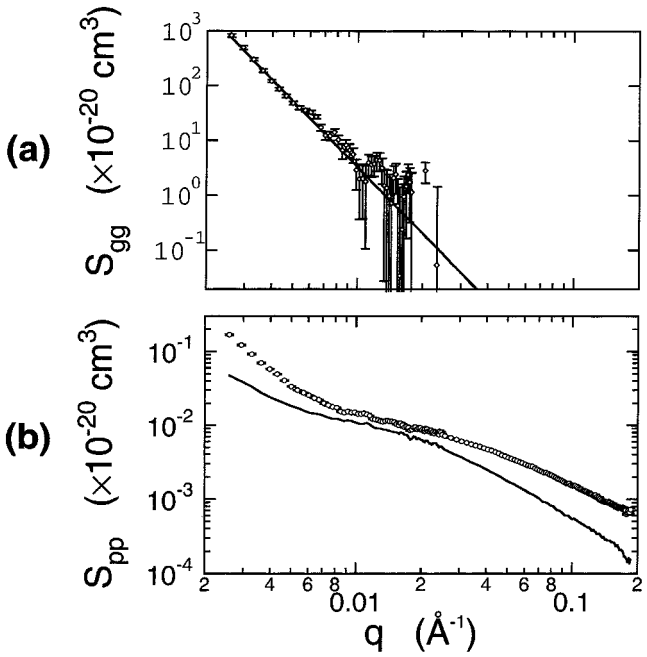

Figure 4. Structure factors obtained by solving eq 7. (a) S_{gg}. This structure factor shows a q^{-4} dependence, as expected for Porod scattering from a surface. (b) S_{pp}. The dominant feature of this structure factor is the Beaucage form due to the solvated polymer. For comparison, the structure factor of the polymer at 7 °C (lower line), scaled to account for the change in volume fraction, is also plotted. The excess scattering exhibited by the 2.5 °C structure factor suggests the presence of an adsorbed layer.

Figure 4a shows the function S_{gg}. The good fit to the Porod law indicates that the contrast variation method has successfully separated the structure factors: nowhere was a Porod law assumed for these data. The Porod fit to $S_{gg}(q)$ yields a surface-to-volume ratio of 5000 cm^{-1}, which is 7 times larger than the surface-to-volume ratio measured in the inhibitor-free case (see Appendix A4). This increase in surface area upon PVP addition is consistent with the observed change in crystal habit from compact octahedra to platelike crystals.[6,33] If we assume the 40:1 aspect ratio mentioned in section I, and a constant amount of hydrate formed, we predict a 13-fold increase in surface area.

Figure 4b shows the polymer structure factor $S_{pp}(q)$. Plotted for comparison is the structure factor of the 7 °C hydrate-free polymer solution from Figure 2, scaled to account for the increased polymer concentration in the decreased volume of solution. This scaling is due to the influence of the second virial coefficient, as shown in eq 8. (Note that only the value of c in the denominator

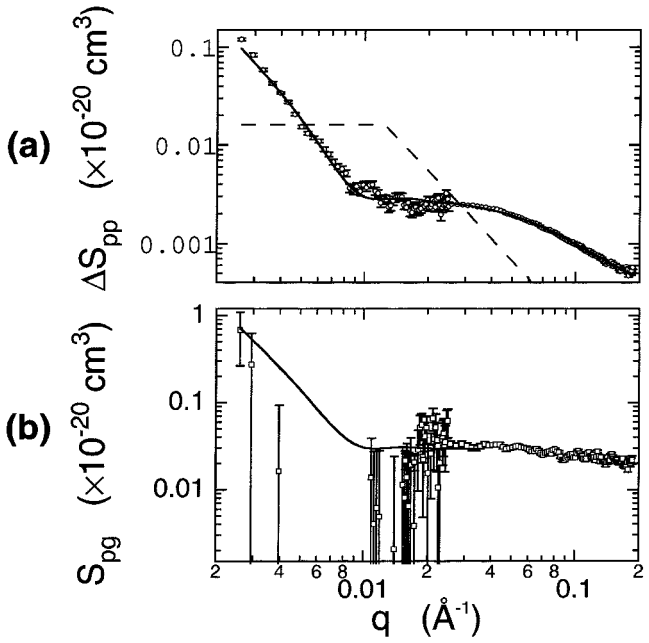

Figure 5. Structure factors for adsorbed polymer layer. (a) ΔS_{pp}. Structure factor S_{pp} after subtracting 99% of the solvated polymer structure factor $\hat{S}_{pp}$. The solid curve shows a fit to a uniform adsorbed layer with high-q scattering due to "blob" scattering. The dashed curve shows the form that would be expected for a self-similar adsorbed layer. (b) S_{pg}. Structure factor S_{pg} (compare with Figure 4). The solid curve shows the fit for a uniform layer with thickness determined in (a), normalized to the data point with lowest q.

is increased—the numerator accounts for the total amount of polymer in the scattering volume, which is unchanged.) The excess scattering evident in S_{pp} clearly indicates the presence of an additional polymer structure, which we attribute to an adsorbed polymer layer. Note that our S_{pp} differs significantly from previous studies where no polymer remained in solution.[21,24] We subtract the contribution of the solvated polymer to obtain ΔS_{pp}, as shown in Figure 5a.

According to the scaling theory of polymer adsorption,[26] adsorbed polymer should form a self-similar layer with a profile described by

$$\phi(z) = (a/z)^{4/3} \tag{9}$$

where a is a length scale on the order of the monomer size and z is the distance from the surface. Note that this form is only valid in the range $R_g^{-1} < q < a^{-1}$. In this q range, scattering from such a layer will have a structure factor given by[21]

$$\bar{S}_{pp}(q) = 2\pi(S/V)(\Gamma V_0)^2 q^{-2}(1 - \sqrt{3}(qa)^{1/3} + f^2(qa)^{2/3}) \tag{10}$$

where V_0 is the monomer volume (which we take to be $\sim a^3$) and $f \approx 4.06a/\Gamma V_0$, which depends on the total surface coverage Γ. Estimating the surface coverage as

$$\Gamma = \frac{1}{a^3}\int_0^\infty \phi(z)\,dz = \frac{1}{a^3}\left(\int_0^a dz + a^{4/3}\int_a^\infty z^{-4/3}\,dz\right) = 4/a^2 \tag{11}$$

for the profile described by eq 9 and approximating $a \approx$ 3 Å yields the dashed curve shown in Figure 5. In the de Gennes model, the layer thickness is set by the single-coil R_g since all adsorbed chains contact the surface at at least one point. Below the value of q corresponding to the layer thickness, we expect a rollover in $\bar{S}_{pp}(q)$ to a constant value. The resulting curve clearly does not fit the measured data. We could adjust the parameters, the monomer size a, and layer thickness h to fit portions of the data. For example, we could fit the high-q region by increasing the value of a to 9 Å and decreasing the layer thickness to 20 Å. These are unrealistic values, and moreover, the resulting curve fails to capture the low-q behavior. Similar changes (in an opposite direction) would move the dashed line near the low-q data but cannot describe the high-q regime.

Table 2. Parameters for the Fit Shown in Figure 5a

parameter	value	units
$S/V \times \phi_s^2$	0.392 ± 0.003	cm^{-1}
h	550 ± 8	Å
ξ	24.8 ± 0.2	Å
d_f	$1.77^a \pm$	
G'	0.00275 ± 0.00001	cm^3

[a] Fixed from fit to S_{pp} (cf. Figure 2).

The simplest alternative is to model the adsorbed polymer as a uniform layer of volume fraction ϕ_s and thickness h. The structure factor for such a layer is[34]

$$S_{pp}^{step} = 4\pi(S/V)\phi_s^2(1 - \cos qh)/q^4 \tag{12}$$

The mass of polymer in the layer is then

$$\gamma = (S/V)h(\phi_s\rho_{poly} + c) \tag{13}$$

per unit sample volume. (Note that $(S/V)hc$ represents the contribution of solvated polymer within the layer volume—we are measuring contrast relative to the polymer solution.) Thus, the fraction y of polymer remaining in solution satisfies $1 - y = \gamma/c$ by mass balance. This form provides an adequate fit to the low-q data. The high-q data in Figure 5a are consistent with "blob" scattering due to density fluctuations within the layer, analogous to that seen from semidilute solutions.[26,35] We model this structure, which corresponds to the term $\tilde{S}_{pp}(q)$ discussed in section III.B, using the Beaucage form (eq 6), constrained to have the same power law as does the free polymer (since we are probing the interior of polymer coils in this regime). The combined fit is shown in Figure 5a with parameters tabulated in Table 2.

If one uses the S/V of the entire crystalline surface (as determined from S_{gg}), we find a surface coverage of $\sigma = h(\phi_s\rho_{poly} + c) = 0.9$ mg/m^2. Although such a total surface coverage is typical of adsorbed polymer layers,[21,36] here it is spread over a thickness of several times R_g, much thicker than that predicted by the standard de Gennes adsorption model.[37] Consequently, the layer concentration would be lower than typical, only about 3 times that in the surrounding solution.

One can overcome this dilemma by relaxing the constraint that the polymer cover all available crystal surface; e.g., S/V in eq 12 can be less than that for eq 3. Figure 5b shows the structure factor S_{gp}, which contains information about adsorbed polymer *alone* (plus an approximately constant background, most likely due to imperfect background subtraction). Overlayed on the data is the structure factor of a step profile

$$S_{pg}^{step}(q) = 2\pi\phi_s(S/V)(1 - \cos qh)/q^4 \tag{14}$$

constrained to pass through the lowest-q data and to have the same value of h found from Figure 5a. The combined fit amplitudes from Figure 5 allow ϕ_s and S/V to be estimated independently. The result is $S/V = 80$ cm^{-1}, about 2% of the total crystalline surface, and $\phi_s = 0.07 \pm 0.04$. This value of ϕ_s corresponds to $\approx 2.5c^*$ and thus describes a layer density high enough for overlapping polymer chains (c^* is the overlap concentration). Admittedly, the data in Figure 5b show a very small signal at low q, resulting in the large uncertainty quoted above, but are clearly not consistent with a large amount of adsorbed polymer. The *local* surface coverage under this assumption is 5 ± 3 mg/m^2.

The fit to the high-q regime of Figure 5a indicates a length scale of 24.8 Å. We take this length to be the mesh size of the semidilute polymer solution within the layer. De Gennes predicts that the mesh size ξ should scale as[37]

$$\xi = a\phi_s^{-3/4} \tag{15}$$

where a is the monomer size. Using the volume fraction in the layer determined above and an approximate monomer size of 3 Å, we expect $\xi \approx 22$ Å. Thus, the high-q part of the structure factor ΔS_{pp} is consistent with the semidilute polymer solution determined through ΔS_{pp} and S_{pg}.

Before proceeding to a discussion of these results, we briefly discuss our confidence in the fits. The error bars shown for the structure factors (Figures 4 and 5) are calculated from the uncertainty, due to counting statistics, in the original scattering data. Not included is the uncertainty in the contrast estimates. These are accurate to within a few percent, with inaccuracy mainly affecting the estimated contrast matching points. Since all of the data are collected in a regime far from the polymer−solvent matching deuteration x_{ps}, errors in the location of this point have little effect on the resulting structure factors measured by the SVD method. Likewise, errors in the crystal-solvent matching point x_{gs} have little effect on S_{gg}—the amplitude of the corresponding parabola in Figure 3 is well defined by data at the end points of our deuteration range. Thus, the surface area is measured to within a few percent by this technique.

The term S_{pg} is more sensitive to uncertainty in x_{gs}. While the existence of an appreciable adsorbed layer is clear from Figure 4b, this layer is not as easily measured in Figure 5b. Thus, while the discussion above of a layer covering only a small fraction of the crystal surface area is in good agreement with the data, the uncertainty estimates indicate only a factor-of-2 confidence in the density of this layer and order-of-magnitude confidence in the fraction of coated surface.

IV. Interpretation

A. Comparison of Noninhibitor and Inhibitor Polymers. As noted in section III.A, comparison of the scattering from polymer plus crystal-slurry samples for noninhibitor and inhibitor polymers shows that they differ in two essential ways: there is a larger Porod amplitude at small q values and an overall higher scattering intensity at large q values for the inhibitor−polymer systems. Furthermore, we had previously noted that the Porod scattering amplitude seems to increase as the effectiveness of the inhibitor increases.[12]

Here, the contrast variation technique has allowed us to separate the scattering into terms specific to crystal surfaces, solvated polymer, and adsorbed polymer. Through eq 2, we estimate the relative importance of these terms to the overall intensity at any given q value. We find that, although the S_{gg} term indicates an approximately 7-fold increase in surface area due to the inhibitor polymer's change of the crystal aspect ratio, the majority of the intensity increase (about 80%) at low q is due to the increase in S_{pp} beyond that due to polymer in solution.

B. Description of the Adsorbed Layer. Before discussing the possible effects of this adsorbed layer on crystal growth, we discuss the nature of the layer itself. One striking feature is its thickness, approximately 7 times R_g. Thus, most of the polymer chains incorporated in the layer do not contact the crystal surfaces. This is in sharp contrast with the de Gennes prediction[37] of self-similar adsorbed layers with no inherent length scales, save the monomer size a and the radius of gyration R_g, which bound the length scales in which this self-similar behavior is predicted. In the de Gennes model, surface adsorption sites are saturated, and all adsorbed chains contact the surface at at least one point.

One possible explanation for the formation of a thick adsorbed layer is aggregation on crystal surfaces. For semidilute solutions, Sun and King[8] use light scattering to measure PVP aggregates with sizes similar to our layer thickness. A possible mechanism of formation for these aggregates is that the solvent quality may depend on polymer concentration in such a way that a local increase in polymer density leads to a poorer (local) solvent, allowing further polymer to join the aggregate.[38] Adsorption of some polymer at the hydrate surface may then induce this self-aggregation. In this scenario, the 550 Å dimension may also measure the aggregate size *along* a surface which is studded with clumps of polymer aggregate.

C. Crystal Growth Inhibition. Our measurement of inhibitor adsorption at the hydrate growth faces, coupled with the knowledge that the inhibitor alters the expression of these faces, suggests that adsorption is fundamental to the inhibition mechanism. Inhibition of crystal growth by impurity adsorption is a well-known phenomenon.[39,40] Additive effects have been studied in the crystallization of ionic crystals, such as sodium chloride,[41] and molecular crystals, such as monosodium glutamate.[42] For faceted crystals, the typical result of such adsorption is to inhibit the growth of specific growth faces, thus altering the growth habit. For example, barium sulfate, a monoclinic crystal, which normally forms plates with {001} faces bounded by {210} edges, can form hexagons bounded by {010} faces when grown in the presence of amino dimethylene diphosphonic acid.[43]

One system that is particularly relevant to our discussion of hydrate inhibition is the growth of ice in the presence of antifreeze glycoproteins (AFGP's).[44] These proteins are produced by polar fish and enable their survival in temperatures below the freezing point of their aqueous body fluids. As with the PVP/hydrate system, significant inhibition of ice growth is seen at concentrations of ~1% AFGP. However, in the case of AFGP's, differential adsorption to differing crystal faces has been measured.[45] The adsorption apparently takes place through specific interactions between repeating units on the protein which match the spacing of water

molecules along the $\langle 01\bar{1}2 \rangle$ direction in ice. This is in contrast with hydrate inhibition by PVP, which does not alter the faces expressed and does not have a repeating group that matches a molecular spacing in the hydrate crystal. To the best of our knowledge, there has been no quantification of the surface density of adsorbed protein.

The hydrate crystals studied here are clearly faceted. Therefore, growth must proceed by the motion of steps with some characteristic height. Type II hydrates can be thought of as an ABC stacking of layers of dodecahedral water cages.[46] The guest molecules, required to stabilize the structure, reside in interlayer hexakaidecahedral cavities. However, neighboring cages share water molecules, so growth cannot proceed by surface diffusion of completed cages to step and kink sites. Most likely growth proceeds by a combined adsorption of guest molecule and water molecules at the edges of steps with a height of two dodecahedral layers (since two layers are needed to enclathrate the guest molecule).

Since faceted crystals grow by step flow,[40,47] with new layers initiated either by 2D nucleation (the birth and spread model) or by continuous production at screw dislocations (spiral growth), growth of such crystals can be inhibited by low concentrations of additives that adsorb preferentially along step edges. Additives that pin the steps thus slow the growth by allowing steps to advance only between additive-adsorption sites. The effective crystallization driving force is then decreased by the line tension of the semicircular step region bounded by the additive sites. Growth can be halted when the impurity density along a step is $\leq 2r^*$, where r^* is the critical (2D) nucleation radius, which represents the smallest radius of curvature that is energetically favorable. Examples of growth inhibition by this mechanism have been discussed in the literature.[39,40,45,48]

We can check whether the measured surface density of adsorbed polymer is sufficient to appreciably inhibit step flow. The density of monomers within $a \sim 3$ Å of the surface (i.e., the density of filled adsorption sites) is

$$a(\phi_s \rho_{poly} + c) N_A / W_{mon} \qquad (16)$$

Thus, we estimate that, within the polymer clumps on the surface, the monomer density is $\approx 0.0015/\text{Å}^2$, corresponding to a spacing (assuming a roughly hexagonal array) of ~32 Å. Note that this spacing is of the order of the mesh size of the layer discussed earlier. Since the hexakaidecahedra are arranged in a hexagonal array with a spacing of ≈7 Å, this corresponds to adsorption at ~20% of available sites. Since typical critical nuclei are of the order of 100−1000 Å across,[49] such a surface density would be sufficient to completely block step flow within the clump. Growth can still proceed between clumps. If we assume that the clumps have roughly the same diameter as their thickness, we estimate a distance between clumps (on a hexagonal lattice) of $l =$ 2300 Å. Such a pinning density would slow growth by a factor of $1 - 2r^*/l$ (see ref 39).

Polymer adsorption probably occurs in the same manner as guest molecule incorporation—by water-molecule caging. This would place the polar pendant group inside partial water cages on the hydrate surface. The remainder of the polymer chain could then interfere with further crystal growth.

A molecular understanding of the interactions between the inhibitor and growing hydrate crystal is not sufficient to explain the resulting change in crystal morphology. Hydrate crystals remain bound by {111} faces whether or not inhibitor is present, yet the inhibitor is able to change the relative growth velocities (and hence relative sizes) of these *crystallographically identical* faces. Thus, the mechanism of differential inhibition of dissimilar growth faces, as described above, does not apply.

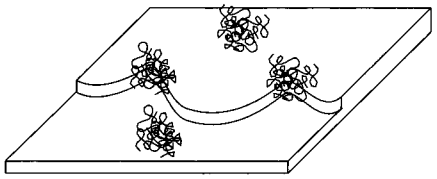

Figure 6. Suggested mechanism of step pinning by adsorbed polymer clumps. Assuming that the clump size is the same as its thickness (550 Å), the 2% coverage implies a distance between clumps of ~2300 Å. The minimum step curvature is determined by the clump spacing. When the spacing is less than the critical 2D nucleation radius, growth must stop entirely.

A possibility is that inhibitor adsorption onto a hydrate growth face slows the growth of that face (e.g., through the mechanism of step pinning described above and in Figure 6). Since all growth faces are identical, the amount of adsorbed polymer is likely to be approximately uniform, resulting in nearly uniform growth. However, small fluctuations in the polymer coverage could result in a spontaneous symmetry breaking: a decrease in the growth velocity of one face will lead to an increased supersaturation at adjacent faces. It has been proposed[6,33] that the increased growth velocity at these faces may prevent the local formation of polymer layers, thus reducing their growth inhibition. The platelike growth is then seen as an instability dependent on both "nutrient" diffusion and a polymer "adsorption time". (The unusual thickness of the aggregate may play a role in slowing the adsorption kinetics.) Note that this mechanism would lead naturally to plate growth—the increase in supersaturation will grow with the number of adjacent faces blocked by inhibitor adsorption. This mechanism would explain the sprouting of plates from apparently random locations on octahedral hydrate crystals when inhibitor is added.[6,33]

The function of a hydrate inhibitor is to allow a hydrate-forming mixture to flow through a pipeline, at hydrate-forming conditions, during a given time interval. Growth inhibition is a likely origin for this ability. As our calculations above suggest, and as has been experimentally observed,[6] the polymeric inhibitors can effectively slow hydrate growth. It is less obvious that the resulting change in crystal morphology, while scientifically intriguing, is a factor during their use as additives. One could speculate that thin crystals might be more easily fractured during flow and thus be less likely to form a solid plug. Of course, inhibitors might also interact with structures in the hydrate-forming solution prior to crystal nucleation.[7] We see no evidence for such an interaction here but have noted increased polymer aggregation in propane/water systems above the hydrate formation temperature.[12]

V. Conclusions

In conclusion, we have used the technique of contrast variation to perform a small-angle neutron scattering measurement of a growth inhibitor, poly(*N*-vinyl-2-pyrrolidone), adsorbed onto crystalline hydrate surfaces.

We deduce an adsorbed layer with the unusual properties of a thickness much larger than the polymer radius of gyration and a profile that does not resemble the standard de Gennes adsorption model. We postulate that the thickness of the layer is due to a polymer self-aggregation effect. Although only portions of the polymer in contact with the growing crystal are likely to affect the crystal growth, it is noteworthy that virtually all effective polymeric hydrate inhibitors exhibit this aggregation.[50]

The contrast variation technique allows us to separate the partial structure factors specific to the crystal interfaces, adsorbed polymer, and excess polymer remaining in solution. We find that the presence of the inhibitor results in a 7-fold increase in the crystalline surface area, in agreement with observations that this inhibitor changes the crystalline growth habit from compact octahedra to a platelike form, thus increasing the surface-to-volume ratio. We find that most (∼99%) of the inhibitor remains in solution. That we are able to measure the scattering from the small amount of polymer that does adsorb is due to the low hydrate-solvent contrast intrinsic to this experiment: Since the crystals are grown in situ from solution, the crystals and solvent have similar compositions and, hence, similar scattering length densities. The polymer, unlike the solutions, is fully hydrogenated and so has a scattering length density very different from that of either the crystal or solvent, resulting in a strong contrast between the crystal and adsorbed layer.

This adsorbed layer is necessarily measured after growth of the crystals is complete. However, since dissolution of polymer layers is slow,[51] the coverage measured is probably indicative of the adsorption during growth. The density of adsorption sites measured is large enough to slow step propagation. (Complete step arrest only requires a spacing of impurities less than the size of the 2D critical nucleus.) Thus, the growth modification may, as has been previously postulated, involve a decreased inhibitor adsorption on fast-growing faces, resulting in a spontaneous symmetry breaking whereby these faces are able to maintain a higher growth rate than the adjacent inhibited faces.

Although this neutron scattering experiment is very sensitive to the presence of adsorbed polymer, it is unable to measure the location of the layer or the precise surface configuration. In order to verify the model described here, a real-space measurement, perhaps by atomic force microscopy, will be necessary.

Acknowledgment. We thank John Huang for suggesting the measurement of surface density by neutron scattering, Scott Milner and Dieter Richter for helpful conversations regarding polymer adsorption and scattering theory, and Alex Levine for aid with programming the singular value decomposition analysis. We acknowledge the NIST Center for Neutron Research and Exxon PRT for providing beamtime and help during the measurements.

Appendix A. SANS Contrast Calculations

To extract quantitative results from scattering data, we need accurate estimates of the contrasts between components of the sample. In neutron scattering, contrasts are typically described in terms of scattering length densities. Since the neutron wavelength is large compared to the molecular (or monomer) sizes, the scattering lengths b_{mol} of the molecules can be calculated as the sum of the atomic scattering lengths:

$$b_{mol} = \sum_{atoms} b_{atom} \tag{A1}$$

Table 3. Molecular Properties of Materials Used in This Study

molecule	mol wt (g/mol)	melt density (25 °C) (g/cm^3)	scattering length[a] ($\times 10^{-12}$ cm)
H_2O	18.0153	0.997	−0.1677
D_2O	20.0274	1.104	1.9153
THF	72.1069	0.886	0.2469
TDF	80.1554	0.985[b]	8.5789
PVP[c]	111.1436	1.264[d]	2.1324

[a] Using data from ref 52. [b] Assuming the same molar density as THF. [c] Sample characterized in ref 8. [d] Effective density in aqueous phase.[53]

Molecular scattering lengths[52] relevant to our experiments are tabulated in Table 3. The scattering length density of a component α can be calculated as the sum of scattering lengths of all molecules in α divided by its volume v:

$$n_\alpha = \frac{1}{v} \sum_{molecules} b_i \tag{A2}$$

We vary the contrast of our solutions, and hence of the resulting hydrates, by varying the deuteration of the water. Since this variation has the effect of substituting H_2O molecules for D_2O's,[54] the scattering length densities vary linearly with the deuterated fraction of water. As a result, the contrasts for the S_{gg} term, $(n_g^{(i)} - n_s^{(i)})^2$, and for the S_{pp} term, $(n_p^{(i)} - n_s^{(i)})^2$, must describe parabolae with minima of zero contrast.

1. Solvent Scattering Length Density. We calculate the scattering length per mole of solvent from the known composition and the molar volume calculated from the mass densities of the components. The molar volume is corrected for the excess volume of mixing, which has been measured for the THF/H_2O system.[55] The composition varies with the amount of solvent frozen into hydrate crystals.

The hydrate crystal has a composition of $17H_2O\cdot g$THF, where g is a filling fraction set by the growth conditions and is approximately equal to 1. We deliberately chose an off-stoichiometric composition to allow partial freezing. Thus, freezing depletes TDF from the liquid fraction. If a mole fraction ϕ of the "water" (D_2O and H_2O) is incorporated into hydrate crystals, then an amount $g\phi/17$ of TDF must also leave solution. We can write the scattering length density of the remaining solvent as

$$n_s = \{(1-\phi)[f_{D_2O}b_{D_2O} + (1-f_{D_2O})b_{H_2O}] + (r - g\phi/17)[f_{TDF}b_{THF} + (1-f_{TDF})b_{TDF}]\}/[W_{H_2O}/\rho_{H_2O} + rW_{THF}/\rho_{THF} + V_{excess}] \tag{A3}$$

where r is the initial mole ratio of THF plus TDF to water, f_{D_2O} is the deuterated fraction of water, the b_α's are the scattering lengths of the various components, the W_α's are the molecular weights, and V_{excess} is the excess volume of mixing. This form explicitly shows the linear dependence of n_s on the deuterated fraction f_{D_2O}. (Recall that the deuterated fraction of THF is fixed at $f_{TDF} = 0.995$.)

We can estimate ϕ using the phase diagram, Figure 1. When an initial solution with a molar fraction $x_0 = 1/(1 + r)$ of TDF is partially solidified, a hydrate with TDF composition $x_s = g/(17 + g)$ and a TDF-depleted solution with a composition x_L given by the phase coexistence curve are formed. By mass conservation, these quantities[56] are related by

$$\phi = \left(\frac{x_0}{1 - x_0} - \frac{x_L}{1 - x_L}\right) \Big/ \left(\frac{x_S}{1 - x_S} - \frac{x_L}{1 - x_L}\right) \quad \text{(A4)}$$

For our samples we estimate a value of $\phi = 0.475 \pm 0.025$ by linearly interpolating between the two curves in Figure 1 to an average deuteration of 0.9.

This value of ϕ corresponds to a solid volume fraction of $\phi_v \sim 0.51$, which is consistent with optical imaging of the slurry samples as well as their dramatic viscosity increase. Since the liquidus line in Figure 1 is quite steep at our experimental temperature, small drifts and errors in temperature will have little effect on this value.

To measure the structure factor of a polymer layer adsorbed onto a crystal surface in the presence of a polymer solution, we must make a slight modification to this scattering length: the appropriate contrast is with the *average solution*, containing THF, water, *and polymer*:

$$\bar{n}_s = \frac{n_s v_s + n_p v_p y_p}{v_s + v_p y_p} \quad \text{(A5)}$$

where v_s and v_p are the molar volumes of the solvent and polymer, respectively, and y_p is the molar ratio of *monomer* to solvent (column 4 in Table 1).

2. Polymer Scattering Length Density. The scattering length density of polymer can be calculated as

$$n_p = N_A \rho_p b_{mon}/W_{mon} \quad \text{(A6)}$$

where N_A is Avogadro's number, ρ_p is the effective polymer density in solution (see Table 3), b_{mon} is the scattering length of a single monomer, and W_{mon} is the monomer formula weight.

3. Hydrate Scattering Length Density. Similarly, the scattering length density of the hydrate crystal phase is calculated as the scattering length of the unit cell divided by the unit cell volume. Thus, we obtain

$$n_g = \frac{136[f_{D_2O} b_{D_2O} + (1 - f_{D_2O}) b_{H_2O}] + 8g[f_{TDF} b_{TDF} + (1 - f_{TDF}) b_{THF}]}{a^3} \quad \text{(A7)}$$

where a is the edge length of the cubic unit cell.

4. Experimental Determination of the Contrast-Matching Points. Not all of the quantities in eqs A3, A6, and A7 are known to the required accuracy. Hence, it is common practice[21] to determine the deuteration fraction x_{gs} where $n_g = n_s$ through experimental measurement. In Figure 7, we plot the amplitudes of Porod fits to the 2.5 °C polymer-free slurry scattering. These amplitudes should describe a parabola with zero minimum at a contrast-matching point x_{gs}. Instead, we find that the data do not reach zero. Because we are assured of a contrast matching point in this deuteration range, this offset implies the presence of some additional scattering. A similar effect is seen by Auvray and Cotton,[21] who attribute it to a thin surface contamination layer. Whatever its origin, provided that its contrast does not vary appreciably with the deuteration fraction of water (i.e., provided that it is both independent of the solvent and has a dissimilar scattering length, as would be expected for a nondeuterated impurity), one can assume that it will contribute an approximately constant "background" and not alter the position of the minimum. Note that the "extra" scattering is quite weak. The Porod amplitude increases dramatically (by a factor of 5−10) when hydrate inhibitor is present, rendering this term unimportant.

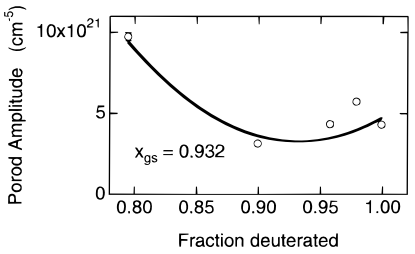

Figure 7. Porod coefficient vs fraction D_2O for the partially frozen polymer-free solvents. The parabolic fit measures a contrast-matching point of $x_{gs} = 0.932$.

The parabolic fit in Figure 7 gives a hydrate-solvent contrast-matching point of $x_{gs} = 0.932 \pm 0.002$. This is an offset from the calculated matching point of 1.023, suggesting that some of the quantities in eqs A3 and A7 are slightly inaccurate. The least well-known quantity is the actual solution density. Although we know the densities of the liquid components and have an estimate of their excess volume of mixing at 25 °C,[55] equivalent data do not exist for the temperatures and deuterated solvents used in our experiment. Thus, we use the experimental matching point to determine the molar volume of the solution to be 19.2 cm^3/mol, 1.2% smaller than our original estimate.

With the hydrate-solvent contrast fixed in this way, we use the fit in Figure 7 to estimate the surface-to-volume ratio of the crystal slurry, through eq 3, to be 700 cm^{-1}. This provides us with an estimate of the crystal sizes: for spherical crystals,

$$\frac{S}{V} = \frac{4\pi r^2 \phi_v}{4\pi r^3/3} = \frac{3\phi_v}{r} \quad \text{(A8)}$$

where the factor ϕ_v represents the volume fraction 0.51 occupied by the crystals. For this simple estimate, we obtain a crystal radius of 22 μm, which is consistent with sizes estimated microscopically for the slurry state.

Using this 1.2% correction to the molar volume of the solution, and eqs A3 and A6, we calculate the polymer−solvent matching point x_{ps} to be 0.160. The variation of fits to the five 7 °C polymer solution data sets shows good agreement with this prediction.

References and Notes

(1) Davidson, D. W. In *Water: A Comprehensive Treatise*; Franks, F., Ed.; Plenum Press: New York, 1973; Vol. 2, pp 115−225.
(2) Kvenvolden, K. A.; Ginsburg, G. D.; Soloviev, V. A. *Geo-Marine Lett.* **1993**, *13*, 32.
(3) Sloan, Jr., E. D. *Clathrate Hydrates of Natural Gases*; Marcel Dekker: New York, 1990.
(4) Lederhos, J. P.; Long, J. P.; Sum, A.; Christiansen, R. L.; Sloan, Jr., E. D. *Chem. Eng. Sci.* **1996**, *51*, 1221.
(5) Patent WO 9532356.
(6) Makogon, T. Y.; Larsen, R.; Knight, C. A.; Sloan, Jr., E. D. *J. Cryst. Growth* **1997**, *179*, 258. Larsen, R.; Knight, C. A.; Sloan, Jr., E. D. *Fluid Phase Equilib.* **1998**, *150−151*, 353.

(7) Sloan, Jr., E. D.; Subramanian, S.; Matthews, P. N.; Lederhos, J. P.; Khokhar, A. A. *Ind. Eng. Chem. Res.* **1998**, *37*, 3124.
(8) Sun, T.; King, Jr., H. E. *Macromolecules* **1996**, *29*, 3175.
(9) Nordmeier, E.; Lechner, M. D. *Macromolecules* **1991**, *24*, 2529.
(10) Smelik, E. A.; King, Jr., H. E. *Am. Mineral.* **1997**, *82*, 88.
(11) Smelik, E. A., personal communication.
(12) King, Jr., H. E.; Hutter, J. L.; Lin, M. Y.; Sun, T. *J. Chem. Phys.*, in press.
(13) Gough, S. R.; Davidson, D. W. *Can. J. Chem.* **1971**, *49*, 2691.
(14) Hanley, H. J. M.; Meyers, G. J.; White, J. W.; Sloan, E. D. *Int. J. Thermophys.* **1989**, *10*, 903.
(15) Tetrahydrofuran-d_8, 99.5 atom % enrichment, lot no. 06806TG; Aldrich Chemical Company, Milwaukee, WI.
(16) Deuterium oxide, 99.9 atom % enrichment, DLM-4; Cambridge Isotope Laboratories, Andover, MA.
(17) As described in ref 12, highly active inhibitors such as PVCap resulted in such anisotropic crystals that it was difficult to produce a uniform slurry, resulting in anisotropic 2D neutron diffraction patterns. This problem was not seen with PVP.
(18) *NG3 and NG7 30-Meter SANS Instruments Data Acquisition Manual*; National Institute of Standards and Technology Center for Neutron Research, 1998.
(19) NIST silica standard B1.
(20) Auvray, L.; De Gennes, P. G. *Europhys. Lett.* **1986**, *2*, 647.
(21) Auvray, L.; Cotton, J. P. *Macromolecules* **1987**, *20*, 202.
(22) Beaucage, G. *J. Appl. Crystallogr.* **1995**, *28*, 717. Beaucage, G. *J. Appl. Crystallogr.* **1996**, *29*, 134.
(23) The procedure is described in: Press, W. H.; Teukolsky, S. A.; Vetterling, W. T.; Flannery, B. P. *Numerical Recipes in Fortran* 77; Cambridge University Press: Cambridge, 1986; Sections 2.6 and 15.4, and was implemented using Mathematica 3.0 (Wolfram Research).
(24) Cosgrove, T.; Heath, T. G.; Ryan, K. *Macromolecules* **1987**, *20*, 2879.
(25) Figure 1 indicates that varying the deuteration will change the solid fraction. Our use of a small (20%) range of H_2O fraction minimizes this effect.
(26) de Gennes, P.-G. *Scaling Concepts in Polymer Physics;* Cornell University Press: Ithaca, NY, 1979.
(27) Higgins, J. S.; Benoît, H. C. *Polymers and Neutron Scattering*; Clarendon Press: Oxford, 1994; Section A3.4.2.
(28) Poppe, A.; Willner, L.; Allgaier, J.; Stellbrink, J.; Richter, D. *Macromolecules* **1997**, *30*, 7462.
(29) Polik, W. F.; Burchard, W. *Macromolecules* **1983**, *16*, 978. Sun, T.; King, Jr., H. E. *Macromolecules* **1998**, *31*, 6383.
(30) Devanand, K.; Selser, J. C. *Nature* **1990**, *343*, 739.
(31) However, the contrast factor for any nondeuterated contamination with scattering length density similar to that of the polymer would show a similar dependence on the deuterated fraction of water.
(32) The presence of both polymer in solution *and* adsorbed polymer (with contrast factors $(n_p - n_s)^2$ and $(n_p - \bar{n}_s)^2$, respectively) requires a fourth contrast column in eq 7. However, the two contrasts are too similar for numerical stability of the SVD method with four unknowns. We simply include the solution structure factor $\hat{S}_{pp}$ as part of S_{pp}.
(33) Larsen, R. *Clathrate Hydrate Single Crystals;* Norwegian University of Science and Technology: Trondheim, 1997 (Ph.D. Thesis).
(34) Auvray, L.; Auroy, P. In *Neutron, X-Ray and Light Scattering*; Lindner, P., Zemb, Th., Eds.; Elsevier: Amsterdam, 1991.
(35) Daoud, M.; Cotton, J. P.; Farnoux, B.; Jannink, G.; Sarma, G.; Benoit, H.; Duplessix, R.; Picot, C.; de Gennes, P. G. *Macromolecules* **1975**, *8*, 804. Witten, T. A. *Rev. Mod. Phys.* **1998**, *70*, 1531.
(36) Barnett, K. G.; Cosgrove, T.; Vincent, B.; Burgess, A. N.; Crowley, T. L.; King, T.; Turner, J. D.; Tadros, Th. F. *Polym. Commun.* **1981**, *22*, 283. Cohen Stuart, M. A.; Cosgrove, T.; Vincent, B. *Adv. Colloid Interface Sci.* **1986**, *24*, 143.
(37) de Gennes, P. G. *Adv. Colloid Interface Sci.* **1987**, *27*, 189.
(38) de Gennes, P.-G. *C. R. Acad. Sci. Paris, Ser. II* **1991**, *313*, 1117.
(39) Tiller, W. A. *The Science of Crystallization: Microscopic Interfacial Phenomena*; Cambridge University Press: Cambridge, 1991. See especially pp 116−128.
(40) van der Eerden, J. P. In *Handbook of Crystal Growth*; Hurle, D. T. J., Ed.; Elsevier: Amsterdam, 1993; Vol. 1, Chapter 6.
(41) Sarig, S.; Glasner, A.; Epstein, J. A. *J. Cryst. Growth* **1975**, *28*, 295.
(42) Sano, C.; Nagashima, N.; Kawakita, T.; Iitaka, Y. *J. Cryst. Growth* **1990**, *99*, 1070.
(43) Davey, R. J.; Black, S. N.; Bromley, L. A.; Cottier, D.; Dobbs, B.; Rout, J. E. *Nature* **1991**, *353*, 549.
(44) Franks, F.; Darlington, J.; Schenz, T.; Mathias, S. F.; Slade, L.; Levine, H. *Nature* **1987**, *325*, 146.
(45) Knight, C. A.; Cheng, C. C.; DeVries, A. L. *Biophys. J.* **1991**, *59*, 409.
(46) Smelik, E. A.; King, Jr., H. E. *Z. Kristallogr.* **1996**, *211*, 84.
(47) Saito, Y. *Statistical Physics of Crystal Growth*; World Scientific: Singapore, 1996.
(48) Kern, R. In *Growth of Crystals*; Sheftal, N. N., Ed.; Consultants Bureau: New York, 1969; Vol. 8. Davey, R. J. *J. Cryst. Growth* **1976**, *34*, 109.
(49) An accurate measurement of the critical nucleus would require values of the latent heat of freezing and the surface energy for the THF−water hydrate system.
(50) Sun, T., private communication.
(51) This property allowed the polymer to be flushed by solvent in ref 21.
(52) Lovesey, S. W. *Theory of Neutron Scattering from Condensed Matter;* Clarendon Press: Oxford, 1984.
(53) Molyneux, P. *Water-Soluble Synthetic Polymers: Properties and Behavior;* CRC Press: Boca Raton, FL, 1983; Vol. 1, p 167.
(54) This assumes that replacing H_2O molecules with D_2O's does not effect the molar densities of solution and does not shift the phase diagram. The results are consistent with this approximation.
(55) Kiyohara, O.; Benson, G. C. In *International Data Series, Ser. B: Thermodynamic Properties of Aqueous Organic Systems. 2a. Excess Volume;* Grolier, J.-P., Ed.; Engineering Sciences Data Unit: 1979.
(56) Note that the quantities $x_\alpha/(1 - x_\alpha)$ are simply the mole ratios of TDF in the various phases.

MA990912P